

MgB₂ Josephson junctions produced by focused helium ion beam irradiation

Cite as: AIP Advances **8**, 075020 (2018); <https://doi.org/10.1063/1.5030751>

Submitted: 25 March 2018 . Accepted: 11 July 2018 . Published Online: 19 July 2018

L. Kasaei, T. Melbourne , V. Manichev, L. C. Feldman, T. Gustafsson, Ke Chen , X. X. Xi, and B. A. Davidson 



View Online



Export Citation



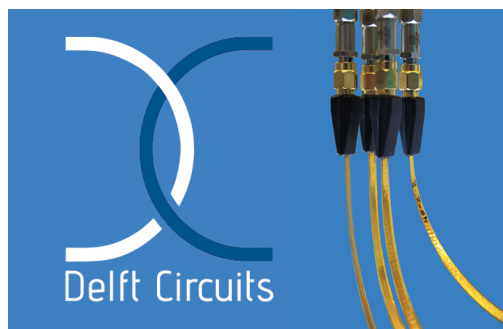
CrossMark

ARTICLES YOU MAY BE INTERESTED IN

[Superconducting nano Josephson junctions patterned with a focused helium ion beam](#)
Applied Physics Letters **113**, 022604 (2018); <https://doi.org/10.1063/1.5042105>

[Direct-coupled micro-magnetometer with Y-Ba-Cu-O nano-slit SQUID fabricated with a focused helium ion beam](#)
Applied Physics Letters **113**, 162602 (2018); <https://doi.org/10.1063/1.5048776>

[Fabrication and characterization of superconducting MgB₂ thin film on graphene](#)
AIP Advances **8**, 075015 (2018); <https://doi.org/10.1063/1.5023658>



Flexible RF Cabling
for Cryogenic Setups

www.delft-circuits.com



MgB₂ Josephson junctions produced by focused helium ion beam irradiation

L. Kasaei,^{1,a} T. Melbourne,^{1,a} V. Manichev,² L. C. Feldman,³ T. Gustafsson,³ Ke Chen,^{1,4} X. X. Xi,¹ and B. A. Davidson^{1,b}

¹Department of Physics, Temple University, Philadelphia, Pennsylvania 19122, USA

²Department of Chemistry and Chemical Biology, Rutgers University, Piscataway, New Jersey 08854, USA

³Department of Physics and Astronomy, Rutgers University, Piscataway, New Jersey 08854, USA

⁴Temple Materials Institute, Temple University, Philadelphia, Pennsylvania 19122, USA

(Received 25 March 2018; accepted 11 July 2018; published online 19 July 2018)

Planar magnesium diboride Josephson junctions are fabricated using focused helium ion beam irradiation. A single track of ion irradiation with a 30 kV He⁺ beam with nominal beam diameter < 0.5 nm is used to create a normal-metal barrier on a MgB₂ film deposited by hybrid physical-chemical vapor deposition. Josephson coupling is observed below the critical temperature of the electrodes for a He⁺ doses between 8x10¹⁵/cm² to 4x10¹⁶/cm². Analysis of the temperature dependence of the normal resistance and critical voltage of the junctions shows highly uniform barriers with nearly ideal resistively-shunted junction behavior for higher-dose junctions, while nonequilibrium effects dominate the properties of lower-dose junctions over most of the temperature range. These results demonstrate that focused helium ion beam irradiation can produce high-quality proximity-coupled MgB₂ Josephson junctions with tailorable properties, promising for use in superconducting devices and circuits. © 2018 Author(s). All article content, except where otherwise noted, is licensed under a Creative Commons Attribution (CC BY) license (<http://creativecommons.org/licenses/by/4.0/>). <https://doi.org/10.1063/1.5030751>

Josephson junctions are crucial elements in a wide range of superconducting devices and circuits.¹ The demand for higher clock speeds in digital circuits has driven impressive advances, in particular in the rapid single flux quantum (RSFQ) technology. RSFQ requires a junction fabrication process that reliably produces circuits with many Josephson junctions and a minimal spread in junction parameters such as critical current density and normal resistance.² Niobium has been the material of choice for the majority of junction applications for decades, and the fabrication process for high quality Nb/AlO_x/Nb trilayer junctions is well established.^{3,4} Other superconducting materials with appealing properties for Josephson junctions have also been investigated. Magnesium diboride (MgB₂), whose superconducting properties were discovered in 2001,⁵ has properties attractive for use in superconducting digital devices. It has a high critical temperature (T_c) of 40 K, the highest among all conventional superconductors. Nb, with a T_c of approximately 9 K, has a practical device operating temperature of 4-5 K, requiring expensive cryogenic cooling with large power consumption. On the other hand, MgB₂ junctions have been shown to operate at as high as 20 K which significantly reduces cooling costs.^{6,7} MgB₂ has two energy gaps ($\Delta_\pi \sim 2.2$ meV and $\Delta_\sigma \sim 7$ meV) both of which are larger than that of Nb ($\Delta \sim 1.5$ meV). This is important for the RSFQ technology as the maximum operating frequency increases with the gap energy. MBE-grown MgB₂/MgO/MgB₂ trilayer junctions have demonstrated Josephson junctions with excellent properties^{8,9} but no information on parameter spreads and reproducibility was given. Similar MgB₂/MgO/MgB₂ trilayer junctions grown by hybrid physical-chemical vapor deposition (HPCVD) have also been reported, but the on-chip spread in

^aL. Kasaei and T. Melbourne contributed equally to this work.

^bCorresponding author email: davidson@temple.edu

critical current density (54%) is too high for practical applications.¹⁰ This could be caused by the growth of the top electrode at high temperature that may degrade the junction barrier. This problem may be alleviated by adopting a planar MgB₂ Josephson junction technology that requires growth of only a single layer of MgB₂.

High energy ion irradiation using neon, oxygen, and other heavy ions (atomic number $Z \geq 18$) at energies >100 keV have been used to produce ion-damaged Josephson junctions in high temperature superconductor YBCO^{11,12} and MgB₂ films.^{13–15} A superconductor film is irradiated through an opening in a mask fabricated by electron-beam lithography, typically ~ 10 nm, which defines the barrier thickness in a planar geometry. The barrier thickness thus produced is several times larger than the in-plane coherence length of $\sim 4\text{--}6$ nm in MgB₂¹⁶ and 2–3 nm in YBCO,¹⁷ severely limiting the values for $I_c R_n$. Decreasing the barrier thickness can increase $I_c R_n$ through the exponential dependence of I_c on thickness. This has led to the use of focused ion beams to restrict the damaged region. For a given substrate and beam diameter, impinging ions with larger atomic number will have larger lateral straggle due to more frequent large-angle scattering events from collisions, resulting in a wider lateral damage region. This suggests the narrowest damaged region will be obtained with low atomic number ion beams such as He⁺ available in a commercial Helium Ion Microscope (HIM). The use of a He⁺ beam to produce Josephson junctions in YBCO has recently been demonstrated.¹² In this paper, we report the properties of high-quality MgB₂ superconductor-normal-superconductor planar junctions with highly uniform barriers made by focused helium ion beam irradiation. 30 nm-thick MgB₂ films are grown on a SiC(0001) substrate by HPCVD; the details of the deposition process have been reported previously.¹⁸ The films are subsequently coated with a bilayer of Cr/Au (5 nm/20 nm) by DC magnetron sputtering to protect the MgB₂ during processing. Standard UV lithography and Ar ion milling are used to pattern an MgB₂ bridge with widths ranging from 2–5 μm . Subsequently, a 300 nm-thick Au film is sputter-coated on the contact pads and the Cr/Au on top of the bridge is removed by Ar ion milling. The sample is then passivated with an 8 nm-thick RF-magnetron sputtered SiO₂ layer.

A Zeiss Orion Plus helium ion microscope is used for irradiation. A single line exposure at room temperature with a 30 kV He⁺ beam (nominal beam diameter < 0.5 nm, pitch = 2 nm) was chosen to form planar SNS Josephson junctions. The range of the 30 kV He⁺ ions in the MgB₂/SiC structure from computer simulations using the TRIM software¹⁹ shown in Fig. 1(a) is greater than ~ 150 nm,

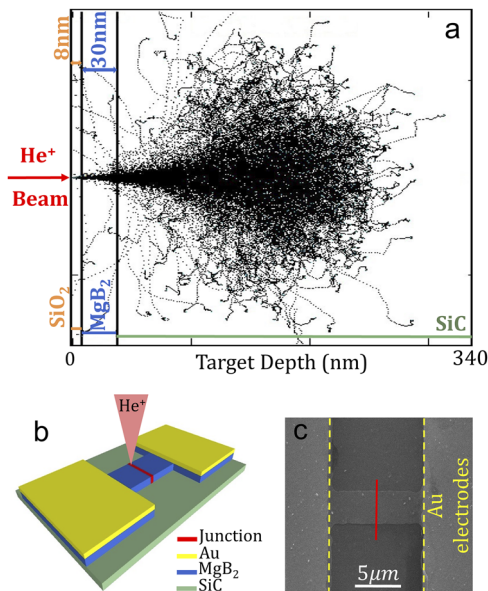


FIG. 1. (a) TRIM simulation showing irradiation of 30 keV He⁺ ions in our film/substrate geometry. Layers (from left to right): 8 nm SiO₂ passivation layer on 30 nm MgB₂ film on SiC substrate. The deduced He⁺ range >150 nm insures that most of the He⁺ ions stop well into the SiC substrate. (b) Schematic of He⁺ beam creating the Josephson junction on a MgB₂ film. SiO₂ layer is not depicted. (c) SEM image of $4 \times 10 \mu\text{m}^2$ bridge. The Helium beam was scanned along the red line.

approximately 4 times the film thickness (30+8 nm). This ensures a minimal lateral straggle of the ions traveling through the MgB₂ film and therefore a more uniform localized damage in the barrier region is obtained. Figure 1(b) shows a diagram of the bridge with the irradiated region indicated in red. The dependence of T_c and normal state resistivity on the He⁺ ion dose have been studied previously on large areas for doses between $10^{13} - 10^{18}/\text{cm}^2$,²⁰ revealing a critical dose of $\sim 8 \times 10^{15}/\text{cm}^2$ for a complete T_c suppression. This dose was taken as the lower limit for the single-track irradiations to produce a barrier for Josephson coupling across the damaged region. Figure 2 shows results for two planar MgB₂ Josephson junctions created with a high dose of $2 \times 10^{16}/\text{cm}^2$ and a low dose of $9 \times 10^{15}/\text{cm}^2$, respectively. Figure 2(a) and (b) show their I - V curves at different temperatures. The Josephson effect is observed in both cases, whereas the critical current density was lower for the high-dose junction ($\sim 1 \times 10^6 \text{ A/cm}^2$ at 4 K) than that of the low-dose junction ($\sim 10^7 \text{ A/cm}^2$ at 4 K). The extremely high J_c of the low-dose junction at low temperature is indicative of a high transparency barrier, as described in the Blonder-Tinkham-Klapwick model.²¹

The I - V curves of the high-dose junction can be fit well by the resistively-shunted junction (RSJ) model for a short junction ($w < 4\lambda_J$, where $\lambda_J = \sqrt{\Phi_0/2\pi\mu_0 d' J_c}$ is the Josephson penetration depth, Φ_0 is the magnetic flux quantum, $d' = d + 2\lambda$ and w is the bridge width) for most temperatures measured, as discussed below. The results are free of hysteresis down to 2.8 K. The low-dose junction displays long-junction behavior ($w > 4\lambda_J$) for $T < 24$ K and the I - V curve becomes hysteretic below 8 K. The I - V curves of planar Josephson junctions are known to deviate from the RSJ model in the long-junction regime due to nonuniform current distribution across the junction,²² consistent with the behavior seen here. Both junctions were exposed to RF radiation at 14.9 GHz in the short-junction regime, i.e. at sufficiently high temperatures. Figures 2(c) and 2(d) show the I - V curves with and without RF radiation at 12 K and 26 K for the high-dose and low-dose junctions, respectively. Shapiro steps are seen in both samples with current steps at voltages corresponding to $nhf/2e$, where n is an integer and f is the frequency of the RF radiation. The Shapiro step height as a function of the RF power is shown for different orders for the high-dose junction in Fig 2(e) and low-dose junction in Fig 2(f). Oscillations expected for the RF Josephson effect was observed in both cases. For the high-dose junction, the steps are seen at all temperatures below T_c , while for the low-dose junction the steps disappear below 8 K, coinciding with the onset of hysteresis in the I - V curve.

Figure 2(g) and (h) show the magnetic field dependence of the junction critical current for the high-dose and the low-dose junctions, respectively. The high-dose junction shows a nearly-ideal Fraunhofer modulation of the critical current with field, however even at the highest measured temperature (14 K) at which the junction should be in the short-junction limit by both criteria

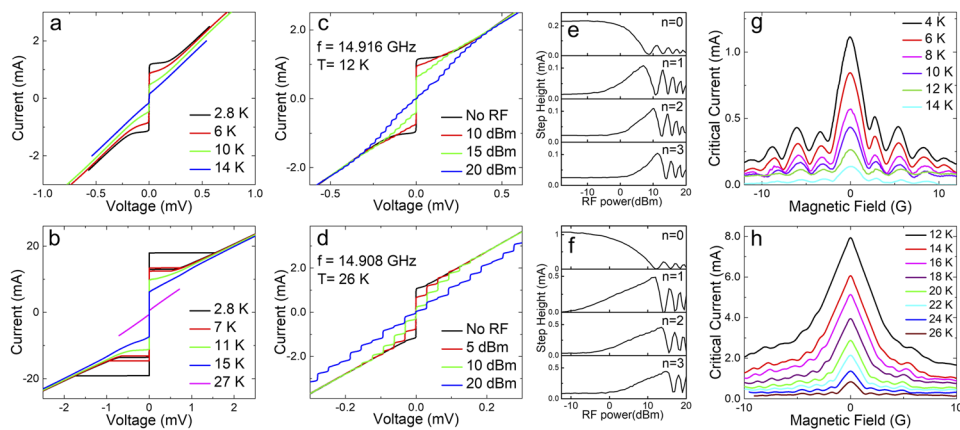


FIG. 2. Magnetotransport measurements for SNS Josephson junctions (JJs) fabricated with high dose ($2 \times 10^{16}/\text{cm}^2$, top row) and low dose ($9 \times 10^{15}/\text{cm}^2$, bottom row). Current-voltage characteristics at different temperatures for (a) high-dose and (b) low-dose JJs. Shapiro steps for (c) high-dose JJ at $T = 12$ K, and (d) low-dose JJ at $T = 26$ K. Microwaves are applied with a frequency of $f = 14.9$ GHz, and height dependence of the zeroth ($= I_c$), 1st, 2nd and 3rd Shapiro steps on applied microwave power are shown (e) for the high-dose JJ at $T = 12$ K, and (f) for the low-dose JJ at $T = 26$ K. Modulation of the critical current as a function of magnetic field at different temperatures are shown in (g) for the high-dose JJ, and (h) for the low-dose JJ.

($w < 4\lambda_J$ and close fit of the I - V curve to the RSJ model, as mentioned above) the lack of complete suppression of critical current and the small deviation from the expected $\sin(x)/x$ shape suggests the barrier is not perfectly uniform. At the lowest temperatures (4–6 K) the pattern evolves toward the characteristic long-junction behavior seen in the lower-dose junction below ~ 24 K, where a linear I_c -vs-field dependence of the primary lobe is seen. This linear dependence is well understood and is due to nucleation of vortices at the junction edge and subsequent flux-flow motion instead of field penetration across the entire junction width as occurs in short junctions.²³ From the critical current density of the junctions and the estimated distance between the two electrodes, λ_J given above can be calculated for the two junctions using the penetration depth of MgB₂.⁵ The resulting λ_J for the low-dose junction varies from 190 nm at 12 K to 450 nm at 26 K and, for the high-dose junction, from 450 nm at 3 K to 1.1 μm at 12 K. Compared to the junction length of 4 μm , this would place the low-dose junction in the long junction regime for the entire temperature range measured (and the high-dose junction in the long junction regime below ~ 12 K), in contradiction with the above-mentioned short-junction RSJ behavior of the low-dose junction seen at 26 K. This contradiction can be explained by considering flux-focusing effects that occur when applying perpendicular magnetic field to a planar thin film.²⁴ Due to the Meissner effect, the electrodes at both ends of the junction barrier push the magnetic field lines into the junction barrier area and therefore the penetration depth of the superconductor thin film calculated by the first I_c minimum (ΔB in the Fraunhofer pattern) is larger than that of the bulk value. Based on the analysis of Rosenthal *et al.* for film thickness smaller than the magnetic penetration depth, the period of modulation in the Fraunhofer pattern is decreased and scales inversely with the square of the junction width.²⁵ ΔB for a 4- μm junction is predicted to be 2.3 G. As seen in Fig. 2(g) and (h), the first I_c minimum occurs at 2.2 G for the high-dose junction (at 14 K) and 1.7 G for the low-dose junction (at 24 K), in good agreement with the prediction. Introducing a flux-focusing factor C into the sinc dependence, $\sin(Cx)/x$ with $x = \pi\Phi/\Phi_0$ and Φ is the applied flux, and fitting the Fraunhofer pattern of the high-dose junction at 14 K, yields a value of $C = 32$, corresponding to an effective junction area of 12.8 μm^2 compared to the actual area of 0.4 μm^2 .

Further information about the barrier properties produced by He⁺ irradiation can be obtained by analyzing the temperature dependence of the junction normal resistance R_n , critical current I_c , and critical voltage $I_c R_n$ for both junctions (Figure 3). Both I_c and R_n were taken from fits of the I - V curves to the RSJ model (with and without excess current, see below). The temperature independence of R_n indicates that the irradiated barrier is fully normal down to 2.8 K for both low- and high-dose junctions and its resistance increases with dose. Taking the normal resistance at 10 K from the large-area irradiation data²⁰ and using the resistivity equation $R = \rho L/A$, we can estimate the barrier length as < 10 nm for both junctions. This is somewhat larger than expected for the sub-nm He⁺ beam used and the lateral straggle taken from the TRIM simulations, and can be considered an upper limit. The critical current increases with decreasing temperature for both junctions. According to Likharev's theory for proximity-coupled junctions,²⁶ for a normal barrier in the dirty limit the temperature variation of the $I_c R_n$ product follows the expression:

$$I_c R_n \propto (1 - t^4) \frac{L\sqrt{t}}{\xi_n(T_c)} \exp\left[-\frac{L\sqrt{t}}{\xi_n(T_c)}\right]$$

Here $t = T/T_c$ is the reduced temperature, L is the barrier length (the electrode separation, referred to earlier as the barrier thickness), and $\xi_n(T_c)$ is the coherence length of the normal metal at the electrode T_c (39 K). (In the clean limit, \sqrt{t} should be replaced by t in this expression.) Fits of $I_c R_n$ versus temperature (Fig. 3) yield values of $L/\xi_n(T_c) \approx 6.2$ for the high-dose and 4.8 for the low-dose junction. This permits an estimate of $\xi_n(T_c) \approx 1.6$ nm for the high-dose and ≈ 2 nm for the low-dose junction. Fitting $I_c R_n$ with the above expression in the clean limit gives similar values.

At high enough critical current (< 15 K for high-dose and < 25 K for low-dose) both junctions show an "excess" critical current, i.e. a nonzero intercept when extrapolating the ohmic portion of the I - V curve (at voltages greater than $\sim 5I_c R_n$). This excess critical current is important for practical operation since it is not completely modulated under applied magnetic field and thus can impact device performance; excess currents can also reveal more fundamental information about nonequilibrium transport in the junction that alters the current-phase relationship. Theoretical treatment of

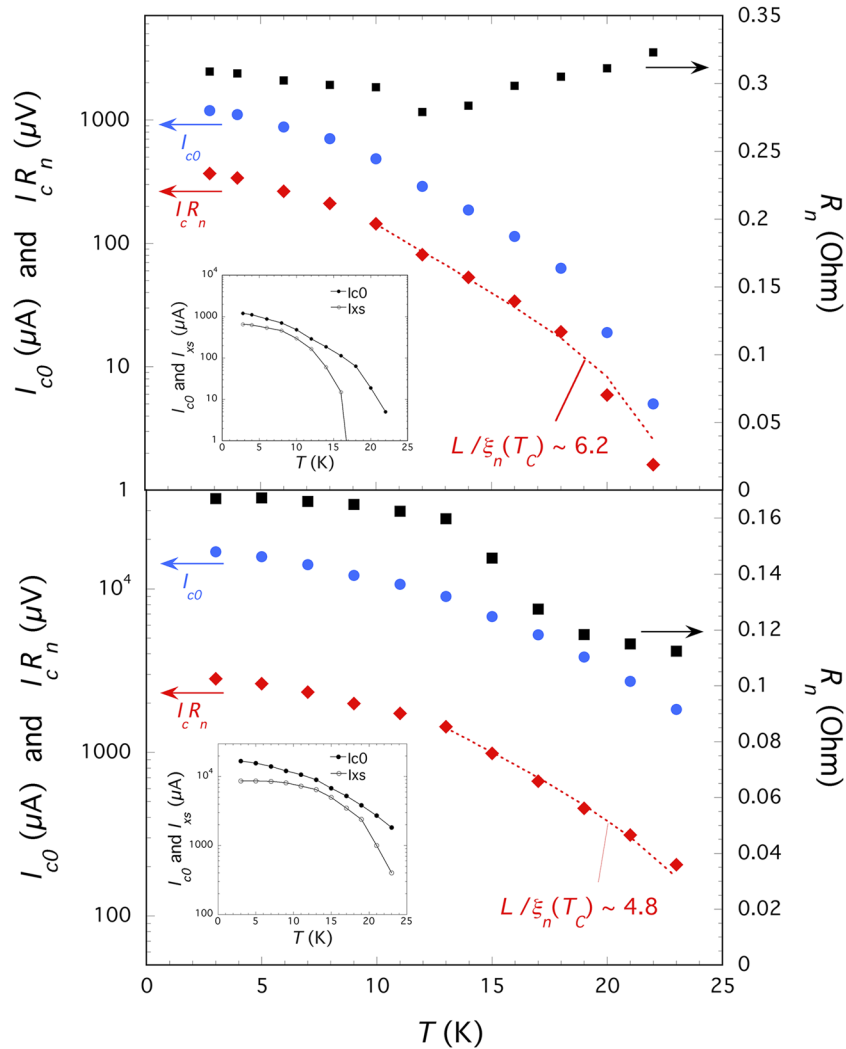


FIG. 3. Temperature dependence of the junction normal resistance (black squares), critical current (blue circles) and critical voltage (red diamonds) for both low- and high-dose junctions. Fits of the $I_c R_n$ to the proximity-coupled expression in the dirty limit described in the text is shown in dashed lines.

nonequilibrium effects in proximity-coupled Josephson junctions is based on the time-dependent Usadel equations²⁶ at high J_c (i.e. low temperature) in which nonequilibrium conditions lead to both excess current, that saturates at $\sim 75\%$ of I_c (in qualitative agreement with the data in Fig. 3 for both junctions at low temperatures), and eventually hysteresis, as seen in the low-dose junction. Strong nonequilibrium effects are expected for high-transparency normal barriers. Excess current and hysteresis can also result from heating (the “hot spot” model²⁷) but these have a power dependence that cannot explain the data in Fig. 3.

In summary, we have fabricated high quality planar MgB₂ SNS Josephson junctions using He⁺ focused ion beam damage to create a normal metal barrier. The two doses studied here, $9 \times 10^{15}/\text{cm}^2$ and $2 \times 10^{16}/\text{cm}^2$, both show Josephson coupling characteristic of a highly uniform barrier. While the high-dose junction exhibits both AC and DC Josephson effects for all the temperatures measured, the AC Josephson effect disappears below 8 K for the lower dose junction, the onset temperature of hysteresis in the I - V curve. The magnetic-field dependence of junction I_c indicates flux focusing effects in the planar thin film limit are important. The high-dose junction shows nearly ideal RSJ behavior in the temperature window between 15 and 25 K, while the high-transparency barrier in the low-dose junction leads to transport properties dominated by nonequilibrium effects over most

of the measured temperature range. These results show that the junction properties such as R_n , I_c and $I_c R_n$ at a desired temperature can be tailored by dose over a range that is useful in a wide variety of superconducting electronic applications. Since writing times are of order milliseconds at these doses in micron-wide bridges, our results suggest that the He⁺ ion damage technique may be useful to prototype e.g. RSFQ circuits requiring hundreds or thousands of junctions with narrow parameter spreads in MgB₂ films operating at or above 20 K.

This work was supported by NSF grant DMR–1310087. L. K. and T. M. acknowledge the Temple Materials Institute for use of their facilities. The scanning electron imaging was performed at Temple in the CoE-NIC facility funded by DoD DURIP Award N0014-12-1-0777 from the ONR and sponsored by the College of Engineering, Temple University.

- ¹ J. Q. You and F. Nori, "Superconducting circuits and quantum information," *Phys. Today* **58**, 42 (2005).
- ² K. K. Likharev and V. K. Semenov, "RSFQ logic/memory family: A new Josephson-junction technology for sub-terahertz-clock-frequency digital systems," *IEEE Trans. Appl. Supercond.* **1**, 3 (1991).
- ³ C. Kaiser, *High quality Nb/Al-AlO_x/Nb Josephson Junctions: Technological Development and Macroscopic Quantum Experiments*, (Vol. 4, KIT Scientific Publishing, 2011).
- ⁴ M. Bhushan and E. M. Macedo, "Nb/AlO_x/Nb trilayer process for the fabrication of submicron Josephson junctions and low-noise dc SQUIDs," *Appl. Phys. Lett.* **58**, 1323 (1991).
- ⁵ J. Nagamatsu, N. Nakagawa, T. Muranaka, Y. Zenitani, and J. Akimitsu, "Superconductivity at 39 K in magnesium diboride," *Nature* **410**, 63 (2001).
- ⁶ D. Cunnane, C. Zhuang, K. Chen, X. X. Xi, J. Yong, and T. R. Lemberger, "Penetration depth of MgB₂ measured using Josephson junctions and SQUIDs," *Appl. Phys. Lett.* **102**, 072603 (2013).
- ⁷ D. Cunnane, K. Chen, and X. X. Xi, "Superconducting MgB₂ rapid single flux quantum toggle flip flop circuit," *Appl. Phys. Lett.* **102**, 222601 (2013).
- ⁸ L. Li, H. Zhang, Y.-H. Yang, and G.-X. Miao, "High-quality epitaxial MgB₂ Josephson junctions grown by molecular beam epitaxy," *Adv. Eng. Mater.* **19**, 160792 (2017).
- ⁹ K. Ueda, S. Saito, K. Semba, and T. Makimoto, "All MgB₂ Josephson tunnel junctions," *Appl. Phys. Lett.* **86**, 172502 (2005).
- ¹⁰ T. Melbourne, D. Cunnane, E. Galan, X. X. Xi, and K. Chen, "Study of MgB₂ Josephson junction arrays and sub- μ m junctions," *IEEE Trans. Appl. Supercond.* **25**, 1 (2015).
- ¹¹ K. Chen, S. A. Cybart, and R. C. Dynes, "Planar thin film YBa₂Cu₃O_{7- δ} Josephson junction pairs and arrays via nanolithography and ion damage," *Appl. Phys. Lett.* **85**, 2863 (2004).
- ¹² S. A. Cybart, E. Y. Cho, T. J. Wong, B. H. Wehlin, M. K. Ma, C. Huynh, and R. C. Dynes, "Nano Josephson superconducting tunnel junctions in YBa₂Cu₃O_{7- δ} directly patterned with a focused helium ion beam," *Nat. Nanotechnol.* **10**, 598 (2015).
- ¹³ K. Chen, Y. Cui, Q. Li, and X. X. Xi, "Study of Planar MgB₂/TiB₂/MgB₂ Josephson junctions using the proximity effect SNS model," *IEEE Trans. Appl. Supercond.* **17**, 955 (2007).
- ¹⁴ D. A. Kahler, J. Talvacchio, J. M. Murduck, A. Kirschenbaum, R. E. Brooks, S. B. Bu, J. Choi, D. M. Kim, and C. B. Eom, "Planar Josephson junctions fabricated with magnesium diboride films," *IEEE Trans. Appl. Supercond.* **13**, 1063 (2003).
- ¹⁵ G. Burnell, D. J. Kang, H. N. Lee, S. H. Moon, B. Oh, and M. G. Blamire, "Planar superconductor-normal-superconductor Josephson junctions in MgB₂," *Appl. Phys. Lett.* **79**, 3464 (2001).
- ¹⁶ M. H. Jung, M. Jaime, A. H. Lacerda, G. S. Boebinger, W. N. Kang, H. J. Kim, E. M. Choi, and S. I. Lee, "Anisotropic superconductivity in epitaxial MgB₂ films," *Chem. Phys. Lett.* **343**, 447 (2001); M. Xu, H. Kitazawa, Y. Takano, J. Ye, K. Nishida, H. Abe, A. Matsushita, N. Tsujii, and G. Kido, "Anisotropy of superconductivity from MgB₂ single crystals," *Appl. Phys. Lett.* **79**, 2779 (2001).
- ¹⁷ S. K. Malik, and S. S. Shah, eds., *Physical and material properties of high temperature superconductors*, (Nova Publishers, 1994).
- ¹⁸ X. X. Xi, "MgB₂ thin films," *Superconductor Science and Technology* **22**, 043001 (2009).
- ¹⁹ J. F. Ziegler, M. D. Ziegler, and J. P. Biersack, *SRIM: the stopping and range of ions in matter* (Cadence Design Systems, 2008).
- ²⁰ L. Kasaei, M. Demir, N. Acharya, P. Bhattarai, V. Manichev, L. C. Feldman, T. Gustafsson, Y. Collantes, E. Hellstrom, K. Chen, X. X. Xi, and B. A. Davidson, in preparation.
- ²¹ G. E. Blonder, M. Tinkham, and T. M. Klapwijk, "Transition from metallic to tunneling regimes in superconducting microconstrictions: Excess current, charge imbalance, and supercurrent conversion," *Phys. Rev. B* **25**, 4515 (1982).
- ²² M. S. Rzchowski and B. A. Davidson, "Supercurrent peaks in planar high-temperature superconducting Josephson junctions," *Phys. Rev. B* **62**, 12455 (2000).
- ²³ A. Barone and G. Paterno, *Physics and applications of the Josephson effect* (Vol. 1, New York: Wiley, 1982).
- ²⁴ A. I. Gubin, K. S. Il'in, S. A. Vitusevich, M. Siegel, and N. Klein, "Dependence of magnetic penetration depth on the thickness of superconducting Nb thin films," *Phys. Rev. B* **72**, 064503 (2005).
- ²⁵ P. A. Rosenthal, M. R. Beasley, K. Char, M. S. Colclough, and G. Zaharchuk, "Flux focusing effects in planar thin-film grain-boundary Josephson junctions," *Appl. Phys. Lett.* **59**, 3482 (1991).
- ²⁶ K. K. Likharev, "Superconducting weak links," *Rev. Mod. Phys.* **51**, 101 (1979).
- ²⁷ W. J. Skocpol, M. R. Beasley, and M. Tinkham, "Self-heating hotspots in superconducting thin-film microbridges," *J. Appl. Phys.* **45**, 4054 (1974).